

Direct molecular simulation of internal energy relaxation and dissociation in oxygen

Cite as: Phys. Fluids **31**, 076107 (2019); <https://doi.org/10.1063/1.5108666>

Submitted: 30 April 2019 . Accepted: 02 July 2019 . Published Online: 30 July 2019

Maninder S. Grover, Erik Torres , and Thomas E. Schwartzentruber



[View Online](#)



[Export Citation](#)



[CrossMark](#)



CAPTURE WHAT'S POSSIBLE
WITH OUR NEW PUBLISHING ACADEMY RESOURCES

[Learn more](#) 

AIP Publishing

Direct molecular simulation of internal energy relaxation and dissociation in oxygen

Cite as: Phys. Fluids 31, 076107 (2019); doi: 10.1063/1.5108666

Submitted: 30 April 2019 • Accepted: 2 July 2019 •

Published Online: 30 July 2019



View Online



Export Citation



CrossMark

Maninder S. Grover, Erik Torres, and Thomas E. Schwartzentruber^{a)}

AFFILIATIONS

Department of Aerospace Engineering and Mechanics, University of Minnesota, Minneapolis, Minnesota 55455, USA

Note: This paper is part of the special issue on Direct Simulation Monte Carlo—The Legacy of Graeme A. Bird.

^{a)}Electronic mail: schwart@umn.edu

ABSTRACT

A variant of the direct simulation Monte Carlo (DSMC) method, referred to as direct molecular simulation (DMS), is used to study oxygen dissociation from first principles. The sole model input to the DMS calculations consists of 12 potential energy surfaces that govern O₂ + O₂ and O + O₂ collisions, including all spin-spatial degenerate configurations, in the ground electronic state. DMS calculations are representative of the gas evolution behind a strong shock wave, where molecular oxygen excites rotationally and vibrationally before ultimately dissociating and reaching a quasi-steady-state (QSS). Vibrational relaxation time constants are presented for both O₂ + O₂ and O + O₂ collisions and are found to agree closely with experimental data. Compared to O₂ + O₂ collisions, vibrational relaxation due to O + O₂ collisions is found to be ten times faster and to have a weak dependence on temperature. Dissociation rate constants in the QSS dissociation phase are presented for both O₂ + O₂ and O + O₂ collisions and agree (within experimental uncertainty) with rates inferred from shock-tube experiments. Both experiments and simulations indicate that the QSS dissociation rate coefficients for O + O₂ interactions are about two times greater than the ones for O₂ + O₂. DMS calculations predict this to be a result of nonequilibrium (non-Boltzmann) internal energy distributions. Specifically, the increased dissociation rate is caused by faster vibrational relaxation, due to O + O₂ collisions, which alters the vibrational energy distribution function in the QSS by populating higher energy states that readily dissociate. Although existing experimental data appear to support this prediction, experiments with lower uncertainty are needed for quantitative validation. The DMS data presented for rovibrational relaxation and dissociation in oxygen could be used to formulate models for DSMC and computational fluid dynamics methods.

Published under license by AIP Publishing. <https://doi.org/10.1063/1.5108666>

I. INTRODUCTION

In this article, we use atomistic-level simulations to study nonequilibrium oxygen dissociation under conditions relevant to hypersonic flight. Predicting the extent of oxygen dissociation in the shock-layer surrounding a hypersonic vehicle is important because dissociation reactions remove thermal energy from the gas, thereby altering the aero-thermo-dynamics of the compressible flow around the vehicle and altering the convective heat flux to the surface. Perhaps most importantly, atomic oxygen produced by dissociation behind the shock wave diffuses through the boundary layer and drives chemical reactions on the surface that erode the heat shield material.

The challenge in developing predictive numerical models is the strong degree of thermo-chemical nonequilibrium and the fact that dissociation is coupled to the internal energy state (rotational and

vibrational energy) of the gas. While the shock wave immediately converts the directed kinetic energy of the free-stream gas into random kinetic energy (represented by the translational temperature T), the rotational and vibrational energies of the gas molecules excite at finite rates with associated time constants, τ_R and τ_V . Experiments have shown that dissociation does not occur until the internal energy (particularly the vibrational energy) of the gas is sufficiently excited.¹ For this reason, computational fluid dynamics (CFD) models for hypersonic flow include a separate vibrational energy equation in order to track the vibrational energy content of the gas at each location in the flow field (represented by the vibrational temperature T_V). The most commonly used dissociation model, introduced by Park,^{2–4} uses a modified Arrhenius formulation where the temperature is replaced by an effective temperature, $T_{\text{eff}} = (T T_V)^\alpha$, where T is the translational-rotational temperature (assumed to be in equilibrium) and typically $\alpha = 1/2$. Developing and validating higher

fidelity models is challenging because internal energy relaxation, dissociation reactions, and internal energy removal due to dissociation are tightly coupled processes. Furthermore, shock wave experiments used for model validation are only able to study the combined effect of such processes and only under a limited set of conditions.

In this work, we use first-principles simulations to investigate the following aspects of nonequilibrium dissociation in oxygen: (i) What are the time constants for vibrational energy relaxation (τ_V) and how do they depend on T ? (ii) What are the effective oxygen dissociation rate coefficients and how do they depend on T ? (iii) How significant are the effects due to non-Boltzmann internal energy distributions on these rate coefficients? (iv) How do all these parameters differ between $O_2 + O_2$ and $O + O_2$ collisions? (v) Finally, how do the predictions from first-principles calculations compare with experimental data and how do the details differ from existing models?

The direct simulation Monte Carlo (DSMC) method, developed by Bird,⁵ allows us to answer these questions. DSMC is a method of directly simulating the physics of the Boltzmann equation, and therefore, no restrictions are placed on local molecular distribution functions; rather, they are a predicted output of the simulation. The DSMC method, combined with recent advancements in computational chemistry and ever increasing computational power, now enables investigation of postshock internal energy relaxation and dissociation processes from first principles.

The first step is to generate potential energy surfaces (PESs), based on quantum mechanical electronic structure calculations, that dictate the forces between atoms required to simulate high energy collisions between species of interest. One approach is then to use such PESs to perform millions of quasiclassical trajectory (QCT)^{6–8} calculations to create databases of internal energy state transition probabilities and state specific dissociation probabilities.^{8–13} These quantities are then used to generate state-to-state models.^{8–13} While this is a powerful approach and is independent of any empiricism, it quickly becomes intractable. For example, when all quantized rovibrational states are taken into account, there are approximately 10^{14} possible state-to-state transitions for $O_2 + O_2$ collisions in the ground electronic state. This necessitates averaging over rotational energies, or more general energy-binning strategies,^{14–19} in order to reduce the number of simulated transitions to a tractable number. It has been shown that the choice of energy-binning strategy can have a noticeable impact on the simulated internal energy relaxation and dissociation rates.^{20–23}

Instead of using an averaged (or binned) state-to-state approach, we use a variant of the DSMC method that was originally proposed by Koura^{24–26} and referred to as classical trajectory DSMC (CT-DSMC). The approach replaces the stochastic collision models used in DSMC with trajectory calculations, where the dynamics of each collision in the DSMC simulation is integrated using an interatomic potential function. Koura's original implementation used the null-collision technique and empirical potential functions. Since then the CT-DSMC method has been used by Bruno *et al.*^{27,28} to study transport properties of molecular oxygen with interaction potentials derived from molecular beam scattering experiments. Additionally, Norman, Valentini, and Schwartzenruber presented a CT-DSMC implementation using the No-Time-Counter (NTC) collision technique⁵ in combination with *ab initio* PESs, resulting in the approach we now refer to as Direct Molecular Simulation

(DMS).^{29,30} Similar to Molecular Dynamics (MD), the sole model input into a DMS calculation is a PES (or set of PESs). The DMS method has been verified to reproduce pure MD simulation results when using the same PES^{29,30} and has been used to study rotational-vibrational energy relaxation³¹ and dissociation^{32–35} in nitrogen. Although Wagner³⁶ proved that Bird's DSMC algorithm converges to a solution of the Boltzmann equation in the limit of an infinite number of particles, to the authors' knowledge this proof did not consider chemically reacting gas mixtures nor multibody interaction potentials. Thus, at this time, no equivalent convergence proof for the CT-DSMC or DMS methods is known to exist.

Recently, DMS has been used to study oxygen dissociation under isothermal conditions, accounting for only $O + O_2$ collisions.³⁷ Here, we present DMS simulations under both isothermal and adiabatic conditions for the full oxygen system, which require 12 *ab initio* PESs to describe all possible $O_2 + O_2$ and $O + O_2$ collisions (corresponding to all possible spin and spatial degeneracies) in the ground electronic state.

The paper is organized as follows. In Sec. II, the DMS algorithm is summarized, the 12 PESs are described with focus on the $O_2 + O_2$ surfaces, and the postprocessing of internal energy is discussed along with a discussion of electronically excited states. In Sec. III A, isothermal and adiabatic DMS calculations are compared. Sections III B and III C present vibrational relaxation and nonequilibrium dissociation rates, respectively, for both $O_2 + O_2$ and $O + O_2$ collisions including comparison with experimental data. Section III D presents the DMS analysis of the full oxygen system using all 12 PESs, and Sec. IV summarizes the conclusions of the research.

II. SIMULATION DETAILS

A. Direct molecular simulation

A description of the DMS method and details of the current implementation can be found in Ref. 30. The basic algorithm is depicted in Fig. 1, and we briefly summarize the method for clarity in this section. Similar to DSMC, DMS is carried out using time steps of the order of the mean collision time (τ_c) and the ratio of particles in the volume to simulated particles in the volume is called the particle weight (W_p). Similar to DSMC, during each time step, particles are first moved without any interaction and afterward a list of randomized particle pairs is formed in each local collision cell, which has dimensions on the order of the local mean free path (λ_c). The NTC algorithm is then used, with an appropriate cross section (σ), to select which particle pairs are to undergo a collision during each time step. However, while standard DSMC methods use cross section models to select particle pairs to undergo various types of collisions (elastic, inelastic, reactive, etc.), the DMS method first uses a hard-sphere cross section to select a conservatively large number of particle pairs for trajectory calculations. Trajectory calculations are then performed using a PES where it is crucial that the maximum impact parameter (b_{\max}) used to initialize the trajectory calculations is consistent with the conservative hard-sphere cross section used in the NTC method,

$$\sigma = \pi b_{\max}^2. \quad (1)$$

It has been shown that the exact value of the maximum impact parameter has no effect on a DMS solution,³⁰ as long as the value is chosen conservatively. In this manner, it is the PES that dictates the

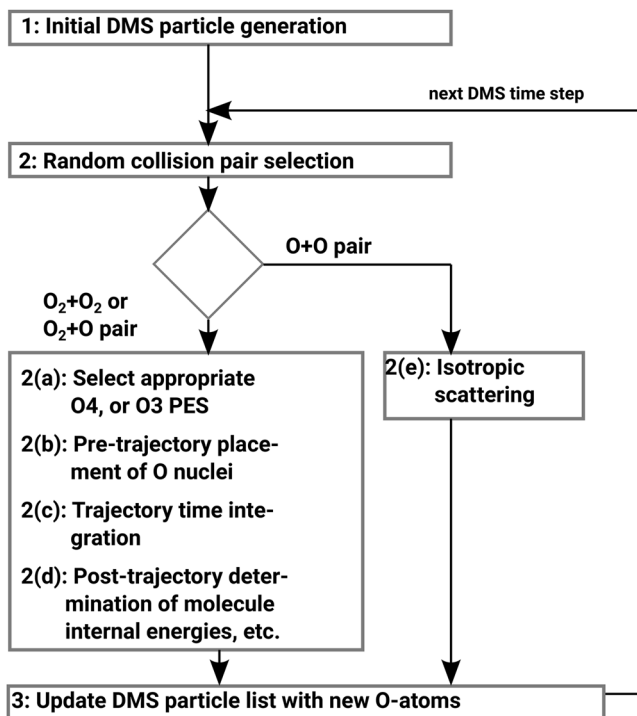


FIG. 1. Zero-dimensional (single-cell) DMS algorithm.

number of elastic, inelastic, and reactive trajectories. For the simulations presented in this paper, the maximum impact parameter is set to $b_{\max} = 6 \text{ \AA}$.

For each trajectory calculation, the phase-space coordinates of all oxygen atoms are then integrated using a velocity Verlet scheme.³⁸ The time step for trajectory integration is set to $\Delta t_{\text{traj}} = 0.5 \text{ fs}$. The trajectory is integrated until the minimum separation between atoms not bound to the same molecule is greater than 15 \AA . It is important to note that the DMS method operates on *atom* positions and velocities. Only as a postprocessing step, precollision and postcollision atomic velocities may be used to determine quantities such as the internal energy of a molecule and the center-of-mass velocity of a molecule. As the internal energy is derived from the atomic velocities and positions, in postprocessing only, there is no decoupling assumed between vibrational energy modes and rotational energy modes within a DMS calculation. During a trajectory, for certain atomic configurations, the atoms may go over local free energy minima in the PES. This may lead to the formation of new bonds and breaking of others. Hence, the DMS method automatically accounts for any type collision outcome, including exchange reactions. If, after a trajectory is completed, atoms belonging to the same molecule are found to be greater than 6 \AA apart, the molecule is considered dissociated. The post-trajectory state of each particle (i.e., the positions and velocities of associated atoms) are then updated in the DMS cell and become the particle's initial state for the next DMS time step.

Since this paper focuses on zero-dimensional in space, isothermal and adiabatic simulations at constant volume, only one DMS

cell is simulated, and particle movement is not needed. The DMS algorithm depicted in Fig. 1 corresponds to such a simplified zero-dimensional calculation. The cell size is such that for the given number of particles, and a density of 1.283 kg/m^3 , the particle weight is unity ($W_p = 1$). The DMS time step is set to values between $\Delta t_{\text{DMS}} = \tau_c/100$ and $\tau_c/10$. Finally, as noted in Fig. 1, atom-atom collisions are not integrated using a PES; rather, a simple isotropic scattering model is used. If desired, a diatomic PES could be used to simulate atom-atom collisions in the DMS method; however, none of the results presented in this article are expected to be sensitive to this procedure.

B. Potential energy surfaces

The predictions of DMS calculations are purely a result of the PES (or set of PESs) that are the only modeling input to the method. In order to study oxygen dissociation, we require surfaces for $O_2 + O_2$ and $O + O_2$ interactions. It turns out that 12 separate PESs are required to model these interactions for the ground electronic state.

Molecular oxygen in its ground electronic state has two unpaired electrons, spin-coupled as a triplet. Hence, an $O_2 + O_2$ interaction can have an overall spin coupling of singlet, triplet, or quintet with statistical weights of these spin couplings being 1, 3, and 5, respectively. Hence, three unique PESs are required to simulate $O_2 + O_2$ interactions. In this work, we use adiabatic *ab initio* PESs developed for the singlet, triplet, and quintet spin coupling of the O_4 system by Paukku *et al.*^{39,40} to fully describe $O_2 + O_2$ interactions in the ground electronic state of the molecules. Additionally, since atomic oxygen in its ground state also has two unpaired electrons, $O + O_2$ interactions can also occur with the total spin coupling being singlet, triplet, or quintet. Furthermore, the spatial symmetry of atomic oxygen generates a threefold degenerate ground state for all three spin states. Hence, due to the spin and spatial degeneracies, nine unique PESs are required to fully describe $O + O_2$ interaction dynamics initiated in the ground states of the collision partners. In this work, we use a suite of nine adiabatic *ab initio* PESs developed by Varga *et al.*⁴¹ to describe the electronically adiabatic collisions of ground electronic-state O_2 with ground electronic-state O . Details of the spin multiplicity and spatial symmetry are beyond the scope of this paper, but more information on group theory, spin multiplicity, and spatial symmetry can be found in Refs. 42 and 43.

Analysis of $O + O_2$ interactions using the PESs of Varga *et al.*⁴¹ can be found in a recent article by Grover *et al.*³⁷ Significant differences between the nine PESs were evident, particularly in the energy barrier (or lack of barrier) for exchange reactions ($O^a + O^b O^c \rightarrow O^a O^b + O^c$), which led to large differences in the vibrational relaxation rate predicted by the different PESs. Specifically, PESs for certain spin and spatial degeneracies that had a low energy barrier for the exchange process produced vibrational relaxation rates approximately 10 times faster than those PESs that had high exchange barriers.³⁷ Since the vibrational relaxation rate is one of the most important quantities we are interested in, this result implies that analysis including all possible spin and spatial degeneracies is necessary. Furthermore, significant differences³⁷ were found between the O_3 PES of Varandas and Pais⁴⁴ and the corresponding O_3 PES of Varga *et al.*,⁴¹ including a large difference in the vibrational relaxation rate. The major difference between the two PESs was shown

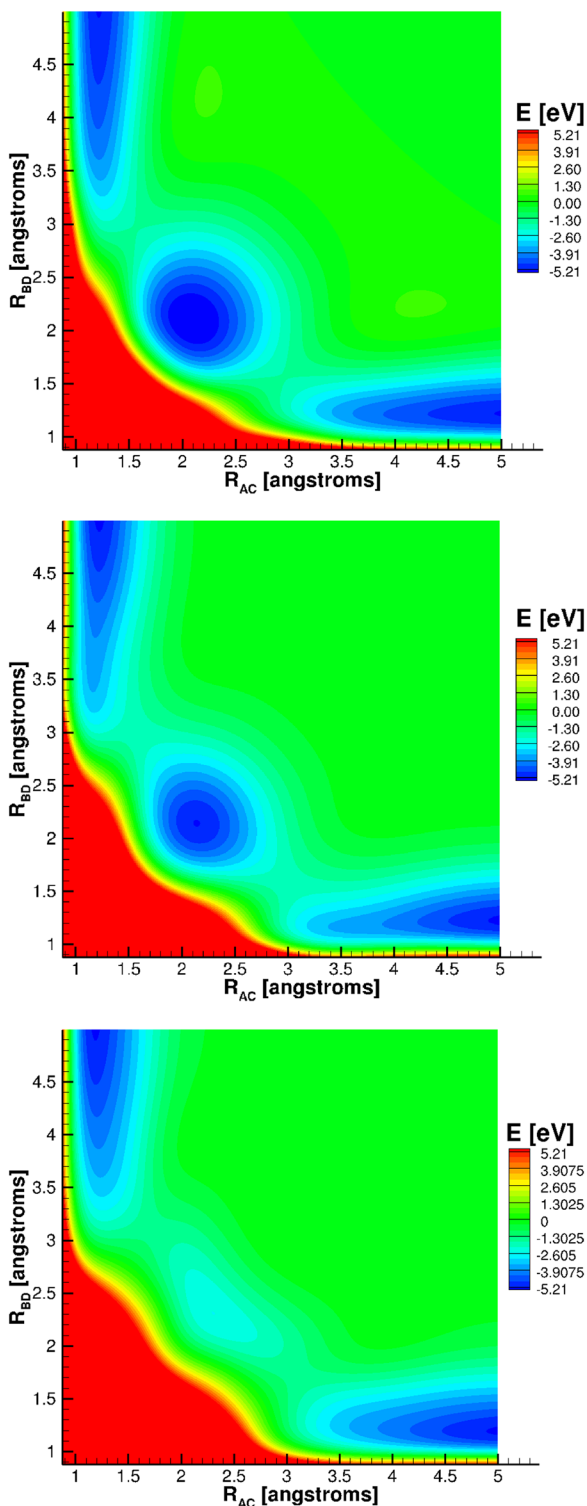


FIG. 2. Energy contours for an in-plane rhombic arrangement of four oxygen atoms produced by the PESs for the three spin states of the O_4 system:^{39,40} O_4 singlet (a), O_4 triplet (b), and O_4 quintet (c).

to be caused by a numerical interpolation artifact in the Varandas PES. Specifically, the Varandas PES contains spurious energy maxima that inhibit the exchange process, and reported results using the Varandas PES predict vibrational relaxation rates approximately one order of magnitude lower than those predicted by the PES of Varga *et al.*³⁷ The O_3 PES of Varandas and Pais⁴⁴ has been used extensively in the hypersonics community to study the properties of $O + O_2$ interactions^{23,45–47} and to propose high quality models.^{48,49} However, the accuracy of these models relies on the underlying PES. Therefore, not only are PESs for each spin and spatial degeneracy required for accurate *ab initio* predictions, but the accuracy of each PES is important as well.

In this article, we now include the three additional PESs required to describe $O_2 + O_2$ interactions.^{39,40} Figure 2 shows energy contours for an in-plane rhombic arrangement of four oxygen atoms produced by the PESs for the three spin states of the O_4 system.^{39,40} To produce this figure, we arrange four oxygen atoms to be in the same plane, with each atom representing a vertex of a quadrilateral $ABCD$ and the point of intersection of the diagonals of the quadrilateral labeled “O.” The inner angles, $\angle AOD = \angle AOB = \angle COD = \angle COB = 90^\circ$, are fixed and distances R_{AC} and R_{BD} are varied. It is observed that when all atoms are far away there is an energy plateau of $E = 0$ eV, and when one or more interatomic distances become small, a repulsive wall is observed. For all three surfaces, product-reactant valleys are observed when R_{AC} is equal to the diatomic equilibrium bond length ($R_{AC} \sim 1.2 \text{ \AA}$) and R_{BD} is large, and similarly when R_{BD} is near the equilibrium bond length and R_{AC} is large. Furthermore, on the O_4 singlet PES, there is an energy valley centered around $R_{AC} \sim 2.2 \text{ \AA}$ and $R_{BD} \sim 2.2 \text{ \AA}$. A similar structure is present in the O_4 triplet PES, but the valley is comparatively shallower and not as wide as it is in the O_4 singlet PES. This feature becomes even weaker on the O_4 quintet PES. These variations are attributed to the difference in electronic arrangements corresponding to each surface. The effect that these different PES features end up having on quantities of interest will be analyzed using DMS calculations in Sec. III.

Table I lists the properties of molecular oxygen obtained from the diatomic potential.

C. Treatment of internal energy

The DMS method operates only on the positions and velocities of atoms. Therefore, no *a priori* assumption involving decoupling vibrational and rotational energy modes is made. As a post-processing step only, the position and velocity of atoms bound within a molecule are used to determine the internal energy of the

TABLE I. Properties of diatomic oxygen from the PES.

Quantity	Value
Diatomc well depth	5.21 eV
Number of vibrational levels	45
Number of rotational levels	241
Number of rovibrational levels	6115
Number of bound rovibrational levels	4581
Number of quasibound rovibrational levels	1534

molecule. In this work, we divide the internal energy of the molecule into vibrational and rotational modes so that our presented results provide an analog for traditionally used terms of vibrational and rotational temperatures.^{2,3}

In our calculations, we split the internal energy using the *vibrational prioritization* framework, as discussed in Ref. 50. When viewed in terms of discrete rovibrational energies, this splitting corresponds to $\epsilon_{vib}(v) = \epsilon_{int}(v, j=0)$ and $\Delta\epsilon_{rot}(v, j) = \epsilon_{int}(v, j) - \epsilon_{int}(v, j=0)$. Here, $\epsilon_{int}(v, j)$ is the discrete internal energy of the molecule, $\epsilon_{vib}(v)$ is the energy in the vibrational mode, and $\Delta\epsilon_{rot}(v, j)$ is the *left-over* internal energy assigned to the rotational mode. This division of internal energy is arbitrary and is one of the several ways one can divide the internal energy of a diatomic molecule.^{6,50}

It should be noted that other than during initialization of a DMS run, the internal energies of DMS molecules practically never correspond to exact values on the rovibrational energy ladder. Even if carefully initialized to a given v, j state, after a single classical trajectory calculation, the internal energies of the molecules involved are no longer quantized and will lie somewhere between the values of the discrete $\epsilon_{int}(v, j)$ -scale. Thus, contrary to the above definitions, the internal energies of molecules during a DMS run practically never populate these states. Instead, during postprocessing, the rotational and vibrational energies of DMS particles are obtained using the procedure outlined in Chap. 16, Sec. 2.5 of Ref. 6. In particular, for a given molecule, we obtain ϵ_{rot} and ϵ_{vib} according to Eqs. (90a) and (90b), respectively. For the purpose of extracting internal energy distributions, we calculate *continuous* rotational and vibrational quantum numbers \tilde{j} and \tilde{v} according to Eqs. (91) and (92) of the same reference. We then simply round to the nearest integer values j and v in order to bin the molecule into a particular rotational and vibrational level. Keep in mind that this approximation is only done during postprocessing and does not modify the atom positions and velocities over the course of the simulations.

The rotational and vibrational energies $\langle\epsilon_{rot}\rangle$ and $\langle\epsilon_{vib}\rangle$ reported in this work represent the averages over all oxygen molecules in the gas at a given time step. We choose to present their evolution normalized by the Boltzmann constant (k_B), so as to yield units of temperature, i.e., $\langle\epsilon_{vib}\rangle/k_B$ and $\langle\epsilon_{rot}\rangle/k_B$. Note that all vibrational energies reported in this paper are measured relative to the minimum of the rotationless O₂ diatomic potential. Thus, all vibrational energies include a zero-point energy of $\epsilon_{int}(v=0, j=0) - \epsilon_{min}(j=0) = 0.0983$ eV. Note also that, as a consequence of our particular separation into rotational and vibrational energies, even at thermal equilibrium in general, $T \neq \langle\epsilon_{vib}\rangle/k_B \neq \langle\epsilon_{rot}\rangle/k_B$. This is the case even as the internal energies of the ensemble of molecules conform to a Boltzmann distribution at T .

Since the PESs used in this work correspond to the ground electronic state, the DMS predictions do not include effects of electronically excited states. However, it is likely that electronically excited states do influence the dissociation process in oxygen. As shown in Table II, there are six electronic states that lie below the dissociation barrier (5.21 eV).⁵¹

A method to account for dissociation from electronically excited states has been proposed by Nikitin,⁵² where it is assumed that the time scale for electronic and vibrational excitation are comparable at high temperatures. In this approach, all electronically excited states are assumed to be in equilibrium, and it is assumed that there will be equilibrium among vibrational levels of the

TABLE II. Electronic states of molecular oxygen and their respective degeneracies.⁵¹

State	Energy (eV)	Degeneracy
$X^3\Sigma_g^-$	-5.21	3
$a^1\Delta_g$	-3.84	2
$b^1\Sigma_g^+$	-3.15	1
$c^1\Sigma_u^-$	-1.02	1
$C^3\Delta_u$	-0.81	6
$A^3\Sigma_u^+$	-0.72	3
$B^3\Sigma_u^-$	1.14	3
$2^3\Pi_g$	1.98	6

electronically excited states. With these assumptions, dissociation would occur concurrently from the ground electronic state and the electronically excited states. An estimate of the overall dissociation rate is then obtained by multiplying the rate from the ground-state calculations by the sum of degeneracies of all the electronic states below the dissociation energy (including ground state) divided by the degeneracy of the ground state. This multiplication factor comes out to be $\eta = 16/3$ for classically bound molecules and has been commonly used in recent work on oxygen dissociation.^{23,45–48} A more accurate method would be to perform electronically nonadiabatic trajectories^{53,54} and to include electronically excited O₂ states explicitly in the DMS simulation. However, this approach requires PESs describing the excited states as well as couplings between states, which are not presently available. Therefore, in this article, when dissociation rate coefficients are presented, we will present the predicted rates from DMS without the factor (i.e., ground electronic state results) and also with the $\eta = 16/3$ factor (i.e., the limiting case where dissociation occurs from all excited states below the dissociation energy).

III. RESULTS

A. Isothermal and adiabatic relaxation simulations

In order to simulate the internal energy relaxation and dissociation processes expected behind strong shock waves with DMS, we perform zero-dimensional isothermal simulations (constant translational energy) and also adiabatic simulations (constant total energy). Results for an isothermal simulation where the translational temperature is maintained at 6000 K and an adiabatic simulation where the gas traverses the temperature range surrounding 6000 K during cooling are shown in Figs. 3(a) and 3(b), respectively. As discussed in the Introduction, we are interested in analyzing the coupling between translational energy (blue line), rotational energy (black line), vibrational energy (red line), and the extent of dissociation (green line). In general, the gas is initialized as pure diatomic oxygen at a high translational temperature and moderate internal temperatures. As the DMS calculation proceeds, the rotational energy mode excites first, followed by the vibrational mode, and the gas begins to dissociate. At longer time scales, these processes all balance and a quasi-steady-state (QSS) dissociation regime is reached. These processes are investigated in detail and compared with available experimental data in Secs. III A–III D.

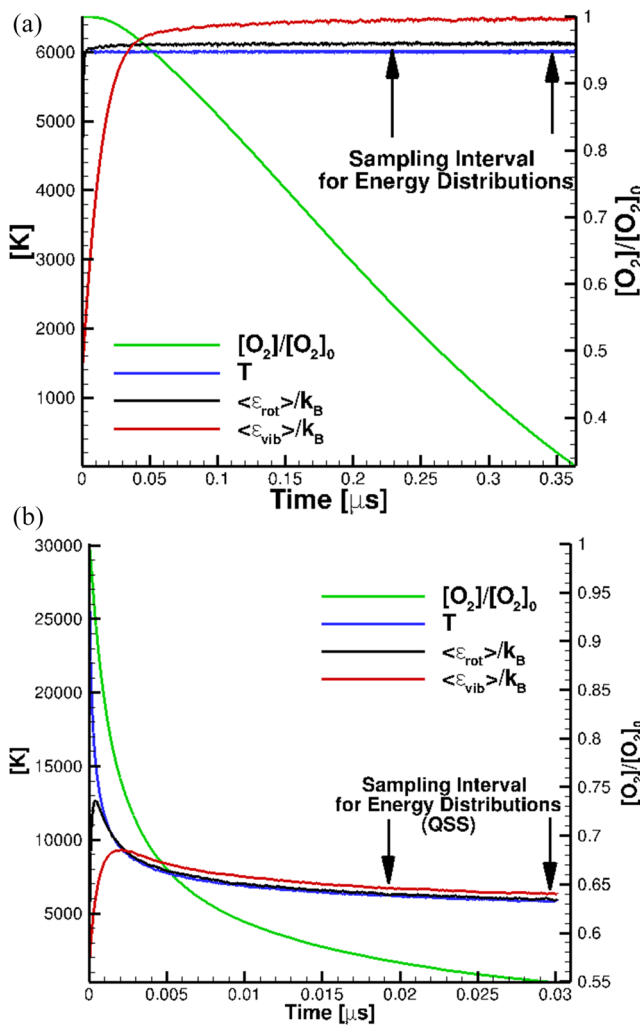


FIG. 3. Profiles of translational temperature (blue), average rotational (black), and vibrational energy (red) normalized by k_B , as well as O_2 concentration (green) for isothermal (a) and adiabatic (b) DMS calculations. Intervals for sampling and time-averaging of internal energy distributions during QSS are delimited by arrows.

The simulations corresponding to Fig. 3 involve both $O_2 + O_2$ and $O + O_2$ interactions using all 12 PESs. As described previously, $O_2 + O_2$ interactions can have an overall spin coupling of singlet, triplet, or quintet with statistical weights of these spin couplings being 1, 3, and 5, respectively. Therefore, during the DMS calculation, each $O_2 + O_2$ trajectory had a 1/9 probability of being integrated using the singlet state PES, 3/9 probability of being integrated using the triplet state PES, and 5/9 probability of being integrated using the quintet state PES. Similarly, there are nine PESs on which $O + O_2$ interactions occur. When an $O + O_2$ pair is selected to undergo trajectory integration, the trajectory has a 1/27 probability to be governed by each of the $1^1A'$, $1^1A''$, $2^1A'$ PESs, a 3/27 probability to be governed by each of the $1^3A'$, $1^3A''$, $2^3A'$ PESs, and a 5/27 probability to be governed by each of the $1^5A'$, $1^5A''$,

$2^5A'$ PESs. For the isothermal case presented here, we started with one million molecules and a total number of 4.8×10^8 molecular trajectories were calculated throughout the entire simulation. By contrast, the adiabatic case used 100 000 initial particles and approximately 1.88×10^8 trajectories were calculated. Recombination is not currently simulated by the DMS method; hence, if the simulation were run for sufficient time, all molecular oxygen would dissociate.

Isothermal simulations enforce a constant translational temperature by resampling the center-of-mass velocities of all particles after each DMS time step from a Maxwell-Boltzmann distribution corresponding to T . This is nonphysical in the sense that energy is constantly being added to the simulation; however, isothermal simulations are useful for inferring relaxation and dissociation rates as a function of T since it remains constant. Many prior DMS and state-resolved studies have been performed using isothermal conditions.^{13,16,20,21,23,32–35,37,55}

Recently, we have extended our DMS algorithm to enable adiabatic simulations by recording the post-trajectory atomic velocities (and corresponding center-of-mass molecular velocities) and using these quantities for the particle's next collision. In this manner, translation energy is converted into internal energy and chemical energy (bond breaking during dissociation). This trend is clearly evident in Fig. 3(b) and is more representative of actual postshock conditions. A recent article describes part of the adiabatic DMS implementation, verifies energy conservation including dissociation, and presents results for nitrogen.⁵⁶

The focus of this section is to answer the following question: How does the vibrational energy distribution function in the QSS dissociating region compare between isothermal and adiabatic simulations? As evident in both Figs. 3(a) and 3(b), a substantial fraction of the dissociation process occurs after the internal energy of the gas is fully excited and the gas appears to be close to thermal equilibrium. Recall, as discussed in Sec. II C, that it is expected that $T \neq \langle \epsilon_{\text{vib}} \rangle / k_B \neq \langle \epsilon_{\text{rot}} \rangle / k_B$. In fact, the internal energy distribution functions may be non-Boltzmann. Therefore, while presenting the average internal energy trends is instructive, it is important to study the internal energy distribution functions within the QSS region. In this QSS region, highlighted in Figs. 3(a) and 3(b), dissociation is removing internal energy from the gas (primarily from the high energy states), while inelastic collisions act to repopulate these high energy states. Both processes balance and the gas reaches a QSS, characterized by non-Boltzmann internal energy distributions where the high-energy tails are depleted compared to a corresponding Boltzmann distribution, as seen in Figs. 4(a) and 4(b). For isothermal simulations, since the translational temperature remains fixed, the QSS distribution is time-invariant. In contrast, for adiabatic simulations, dissociation also removes translational energy from the gas, and it is possible that the QSS distribution function, at a specific temperature T , does not exhibit the same degree of depletion as the corresponding isothermal simulation at T .

It is important to keep in mind that, since the DMS method operates only on the positions and velocities of atoms, the rotational and vibrational modes are naturally coupled. As discussed at the beginning of Sec. II C, any splitting into such modes for plotting purposes is to some degree arbitrary and obtaining *pure* vibrational or rotational energy distributions is impossible. We should therefore clarify that the normalized vibrational populations

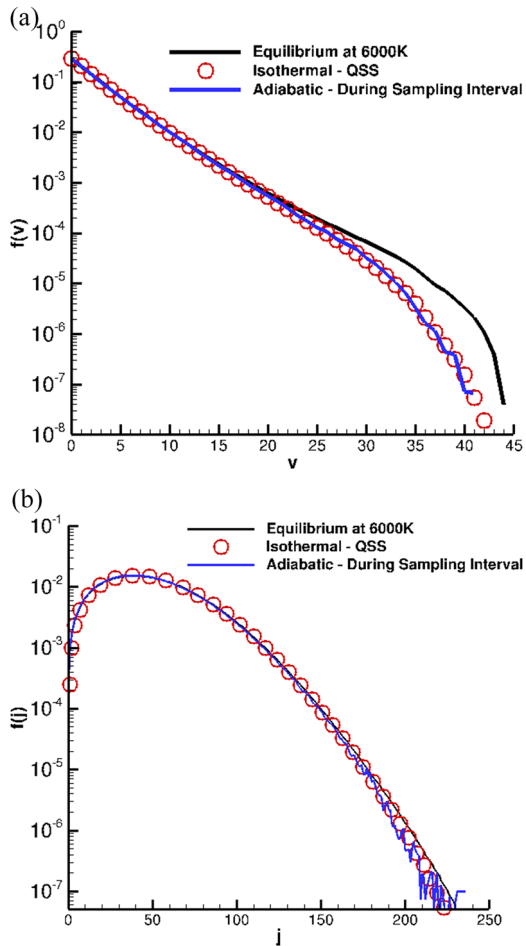


FIG. 4. Comparison of fractional level populations in vibrational (a) and rotational (b) modes during QSS under adiabatic (blue line) and isothermal (red circles) calculations. Boltzmann distribution at 6000 K (black line) shown for reference.

plotted in Fig. 4(a) are actually obtained from *cumulative* populations over all 241 rotational levels of the oxygen molecule, i.e., $f(v) = \sum_j \{n_{O_2}(v,j)\}/n_{O_2}$. Conversely, the rotational populations shown in Fig. 4(b) represent *cumulative* populations over all corresponding 45 vibrational levels of O_2 , i.e., $f(j) = \sum_v \{n_{O_2}(v,j)\}/n_{O_2}$. The vibrational energy distributions plotted in the remainder of this paper [see Figs. 5(b), 10, and 14] use this convention and the vibrational energy $e_{vib}(v)$ on the abscissa follows the definition of Sec. II C.

In order to investigate the QSS distributions, all particle properties are recorded within the isothermal DMS calculation between $t = 0.12 \mu s$ and $0.16 \mu s$ [highlighted in Fig. 3(a)] and in the adiabatic DMS calculation between $t = 0.02 \mu s$ and $0.03 \mu s$ [highlighted in Fig. 3(b)]. In the isothermal case, the translational temperature remains constant at 6000 K, and in the adiabatic case, the translational temperature varies between $T = 6160$ K and 5840 K. In both cases, the average rotational and vibrational energies appear to be in a quasi-steady-state. The QSS distributions for vibrational and

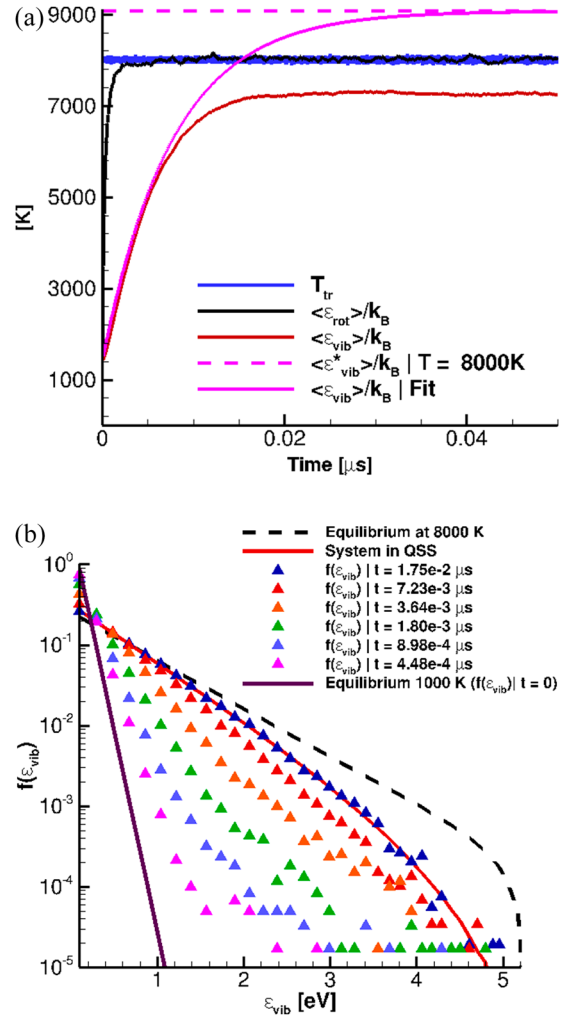


FIG. 5. Example of an excitation calculation for $O_2 + O_2$ interaction. (a) Composition and temperature evolution for an isothermal excitation simulation, where $T_{tr} = 8000$ K. (b) Evolution of the vibrational distribution function for the case shown in Fig. 5(a). Solid purple line shows the Boltzmann distribution at 1000 K, the dashed black line shows Boltzmann distribution of molecules 8000 K, and the solid red line shows the final distribution with a depleted tail due to dissociation. Instantaneous vibrational energy distributions during excitation represented by color-coded triangles.

rotational energy are plotted in Fig. 4. One can see from Figs. 4(a) and 4(b) that the QSS distributions are depleted at the high energy tail of the distribution in comparison with the equilibrium distributions at the given temperature. The depletion is much more pronounced in the vibrational energy distribution compared to the rotational energy distribution, a trend also observed for nitrogen dissociation.^{32–35,37} The important new finding is that the QSS internal energy distribution functions agree almost precisely between isothermal and adiabatic simulations (shown here at a translational temperature of approximately 6000 K). This result indicates that, downstream of a strong shock-wave, as the gas dissociates and thermally cools, it does so through a series of QSS states where internal

energy distributions are non-Boltzmann. Furthermore, these series of QSS states are consistent with those obtained using isothermal calculations corresponding to the local temperature T . Similar agreement between QSS distribution functions in both isothermal and adiabatic DMS calculations was recently found for nitrogen dissociation.⁵⁶ In Secs. III B–III D, we analyze vibrational relaxation time constants and nonequilibrium dissociation rate constants using isothermal DMS calculations and compare simulation predictions to experimental data.

B. Vibrational relaxation

As seen in Fig. 3(a), under isothermal conditions a large degree of vibrational energy excitation occurs before significant dissociation begins. For this reason, we first analyze vibrational energy relaxation due to $O_2 + O_2$ interactions only. To perform such analysis, isothermal DMS calculations were performed in which any atomic oxygen produced as a result of dissociation was simply removed from the simulation. In this manner, internal energy transitions and dissociation reactions are specific to $O_2 + O_2$ interactions only. Furthermore, in addition to simulations using all three PESs (for all three spin couplings governing $O_2 + O_2$ collisions), simulations are performed using only a single PES, corresponding to each of the three individual spin-couplings.

Figure 5 shows the DMS result for an isothermal simulation for the O_4 system. In this case, molecules are initialized such that $\langle \epsilon_{vib} \rangle / k_B = \langle \epsilon_{rot} \rangle / k_B = 1400$ K and the translational temperature is set to 8000 K. The progression of the average energies is shown in Fig. 5(a).

In order to calculate the characteristic vibrational excitation time, the initial portion of the vibrational temperature history is fit using the Landau-Teller expression,⁵⁷

$$\langle \epsilon_{vib} \rangle(t) = \langle \epsilon_{vib}^* \rangle - \Delta(\epsilon_{vib})(\exp(-t/\tau)). \quad (2)$$

Here, $\langle \epsilon_{vib}^* \rangle$ is the final steady-state average vibrational energy, $\Delta(\epsilon_{vib})$ is the difference between the initial and final average vibrational energies, and τ is the characteristic vibrational relaxation time. To calculate the characteristic vibrational relaxation time, $\langle \epsilon_{vib}^* \rangle$ is set to the average vibrational energy under equilibrium conditions at the reservoir temperature T_{tr} . For example, for the case shown in Fig. 5, $\langle \epsilon_{vib}^* \rangle$ is the integral of the equilibrium vibrational energy distribution at 8000 K, shown as the pink dashed line in Fig. 5(a). Only the initial part of the vibrational temperature profile is fit to the above expression in order to eliminate any coupling between vibrational relaxation and energy lost due to dissociation. This fit for the example case is shown as the pink curve in Fig. 5(a).

DMS calculations provide insight into the internal energy excitation process at the molecular level as well. Figure 5(b) shows the evolution of the vibrational energy distribution function for the case presented in Fig. 5(a). The system starts with an equilibrium vibrational energy distribution corresponding to $T = 1000$ K which gives $\langle \epsilon_{vib} \rangle / k_B|_{t=0} = 1400$ K and gradually evolves to the QSS distribution. The mechanism of vibrational energy excitation is similar to that previously observed for nitrogen^{34,35} and for $O + O_2$ interactions.³⁷ As the excitation process begins, the high energy tail of the distribution becomes overpopulated compared to an equilibrium distribution. As the system evolves, the full vibrational energy manifold becomes populated and eventually becomes time-invariant in

the QSS regime, where the QSS distribution shows depletion of high-energy levels. The $O_2 + O_2$ results, shown in Fig. 5(b), are qualitatively similar to previous results for $O + O_2$ processes. However, the deviation from equilibrium (Boltzmann) distributions during excitation due to $O_2 + O_2$ interactions [Fig. 5(b)] is not as severe as that observed for $O + O_2$ interactions.³⁷ This can be attributed to the fact that $O + O_2$ interactions allow for more exchange reactions than $O_2 + O_2$ interactions,⁵⁸ and such exchange reactions are efficient at redistributing internal energy.^{37,59} Singh and Schwartzenruber have proposed a simple model for such overpopulated and depleted internal energy distributions,⁶⁰ which can be used to account for non-Boltzmann effects in continuum CFD models.

Characteristic vibrational relaxation time constants are calculated, specific to $O_2 + O_2$ interactions, for temperatures ranging from 5000 K to 12 000 K. Figure 6 compares the overall characteristic relaxation time constant to the time constants calculated using each individual PES, specific to the individual spin couplings of the O_4 system. We see that vibrational relaxation is fastest for the quintet PES and slowest for the triplet PES. The differences in vibrational relaxation due to individual PESs diminish with increasing temperature. It should be noted that the difference in relaxation time due to individual PESs for $O_2 + O_2$ interactions is not as substantial as observed for $O + O_2$ interactions, where relaxation times varied by over an order of magnitude for the different spin-spatial configurations.³⁷ This is consistent with the finding that vibrational relaxation due to molecule-molecule interactions is dominated by inelastic collisions and involves few exchange reactions.⁶¹ In contrast, relaxation due to molecule-atom interactions is largely influenced by exchange reactions and, hence, spin-spatial configurations that enable exchange reactions lead to faster vibrational relaxation compared to spin-spatial configurations that lack exchange channels.³⁷

For $O_2 + O_2$ interactions, the upper portion of Fig. 7 compares the characteristic relaxation time constants predicted in this study by DMS to those inferred experimentally by Losev and Generalov⁶³ (black circles), Streicher *et al.*⁶⁵ (black inverted triangles), and Ibraguimova *et al.*⁶² (black diamonds). DMS predictions (filled

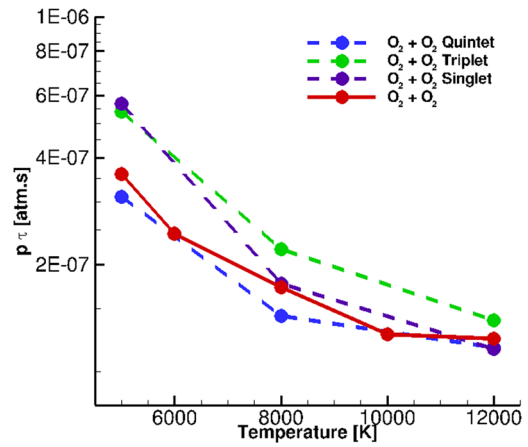


FIG. 6. Comparison of vibrational excitation time among O_4 PESs by Paukku *et al.*^{39,40}

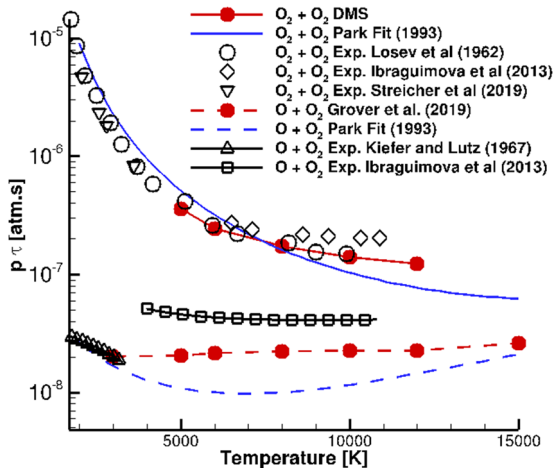


FIG. 7. Comparison of vibrational excitation time obtained for $O_2 + O_2$ interactions with experimental data^{62,63} and results calculated for $O + O_2$ interactions calculated in earlier work³⁷ and experimental results for $O + O_2$ interactions.^{62,64}

red circles on solid line) agree well with the experimental data by Losev and Generalov⁶³ over the temperature range studied. Characteristic relaxation times predicted by DMS match well with the data from experiments by Ibraguimova at lower temperatures but deviate slightly at higher temperatures. The experimental results by Streicher *et al.*⁶⁵ do not overlap with the temperature range studied in this article but follow a similar trend as the DMS data. Figure 7 also includes a comparison with the model proposed by Park² (solid blue line), which is based on the experimental data from the work of Millikan and White.⁶⁶ It can be seen that the Park model deviates from the other results at high temperatures.

For $O + O_2$ interactions, the lower portion of Fig. 7 shows results from earlier work³⁷ (filled red circles on dashed line). It is clear that vibrational relaxation due to $O + O_2$ interactions is more than an order of magnitude faster than that due to $O_2 + O_2$ interactions. As detailed in Ref. 37, $O + O_2$ interactions involve frequent exchange reactions that result in more rapid vibrational energy relaxation. The DMS predictions are seen to agree at low temperatures with the experimentally inferred relaxation rates of Kiefer and Lutz⁶⁴ (black triangles on solid line) and also exhibit a constant trend with increasing temperature in qualitative agreement with experimentally inferred rates of Ibraguimova *et al.*⁶² (black squares on solid line). Also included in Fig. 7 is the model proposed by Park (dashed blue line), which was fit to the low-temperature experimental data of Kiefer and Lutz⁶⁴ with a high-temperature trend that maintains realistic relaxation rates. DMS predictions agree reasonably well with the available experimental data but have a noticeably different trend compared to the widely used Park model.

C. Nonequilibrium dissociation

In this section, we begin by studying the dissociation of oxygen due to $O_2 + O_2$ interactions in the QSS region. The same DMS calculations, where oxygen atoms produced by dissociation are removed

from the simulation, are used to study dissociation rates corresponding to $O_2 + O_2$ interactions only. Isothermal calculations are carried out for the O_4 system for temperatures ranging from 5000 K to 12 000 K. Once the system reaches QSS, nonequilibrium dissociation rates are calculated by fitting the composition history of the system to the equation

$$\frac{d[O_2]}{dt} = -k_d^{O_4}[O_2]^2 - k_d^{O_3}[O][O_2]. \quad (3)$$

Since oxygen atoms produced by dissociation reactions are removed from the simulation, Eq. (3) reduces to

$$\frac{d[O_2]}{dt} = -k_d^{O_4}[O_2]^2. \quad (4)$$

Figure 8 presents the dissociation rate coefficients obtained by DMS calculations during QSS dissociation. The results are plotted for the limiting cases where the multisurface factor is set to $\eta = 1$ (assuming no dissociation from electronically excited states) or it is set to $\eta = 16/3$ (assuming dissociation occurs from all electronically excited states below the dissociation energy). Figure 8 compares the dissociation rate coefficients obtained in this study with the experimental data from the work of Ibraguimova *et al.*⁶² and new data from the work of Streicher *et al.*⁶⁵ Clearly, DMS predictions agree closely with the experimental data when the full multisurface factor ($\eta = 16/3$) is assumed. This suggests that in the experiments the low-lying excited states of O_2 are fully populated. For this reason, we have chosen to report all DMS-derived dissociation rate coefficients in Figs. 8, 9, 11, and 12 including this multisurface factor ($\eta = 16/3$). Ongoing research involves generating PESs for the relevant electronically excited states of oxygen and performing nonadiabatic dynamics calculations to predict the rate of electronic excitation and populations of excited states behind strong shock waves. However, direct experimental evidence of excited state populations is not currently available. Therefore, the results plotted in

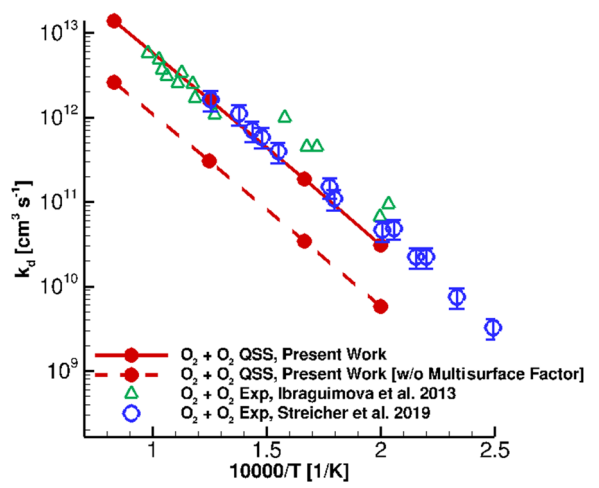


FIG. 8. Comparison of dissociation rate coefficients obtained in this study with the experimental data from the work of Streicher *et al.*⁶⁵ and Ibraguimova *et al.*⁶²

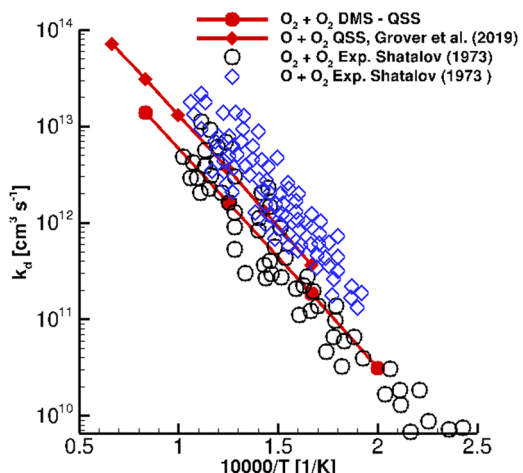


FIG. 9. Comparison between dissociation rate coefficients for O_2 due to $O_2 + O_2$ and $O + O_2^{37}$ interactions obtained by the DMS and experiments by Shatalov.⁶⁷

Fig. 8 only provide indirect evidence that the excited states of oxygen are populated, corresponding to use of the full multisurface factor ($\eta = 16/3$). When compared with the rate coefficients obtained by Ibraguimova *et al.*,⁶² the DMS data agree well at high temperatures but exhibit noticeable discrepancy below 6000 K. However, the DMS data are in close agreement with the recent experimental data of Streicher *et al.*⁶⁵ across the full range of temperatures studied.

In Fig. 9, the DMS results are compared to the dissociation rate coefficients derived from the shock tube measurements made by Shatalov,⁶⁷ where rates for both $O_2 + O_2$ and $O + O_2$ were inferred. While the experimentally obtained rate coefficients have substantial uncertainty, there is a noticeable trend that dissociation proceeds faster when atomic oxygen is present, compared to when the gas is composed of mainly molecular oxygen. DMS results corresponding $O + O_2$ collisions, previously reported in Ref. 37, are plotted in Fig. 9 along with the DMS results corresponding to $O_2 + O_2$ collisions. The DMS calculations also predict faster dissociation in QSS when $O + O_2$ collisions are included by a factor of approximately two. This is in qualitative agreement with the experimental data. Analysis of the vibrational energy distribution function during QSS dissociation, predicted by DMS, clearly shows that the increased dissociation rate is a non-Boltzmann effect.

Figure 10 shows the vibrational energy distribution functions (in QSS) for both the O_4 system and O_3 system DMS calculations. Clearly, the vibrational energy distribution for the O_4 system exhibits greater depletion of the high energy states compared to that found for the O_3 system. This is caused by exchange reactions (frequent in $O + O_2$ collisions⁶¹) that increase the vibrational relaxation rate (refer to Fig. 7) and act to repopulate the high-energy levels.^{68–70} A higher population of vibrationally excited molecules results in the higher QSS dissociation rate constant (Fig. 9) when substantial atomic oxygen is present. Therefore, DMS analysis for both O_3 and O_4 systems, combined with experimental data, provides indirect validation of the non-Boltzmann QSS distribution and its quantitative effect on the dissociation rate constant. It is important to note that

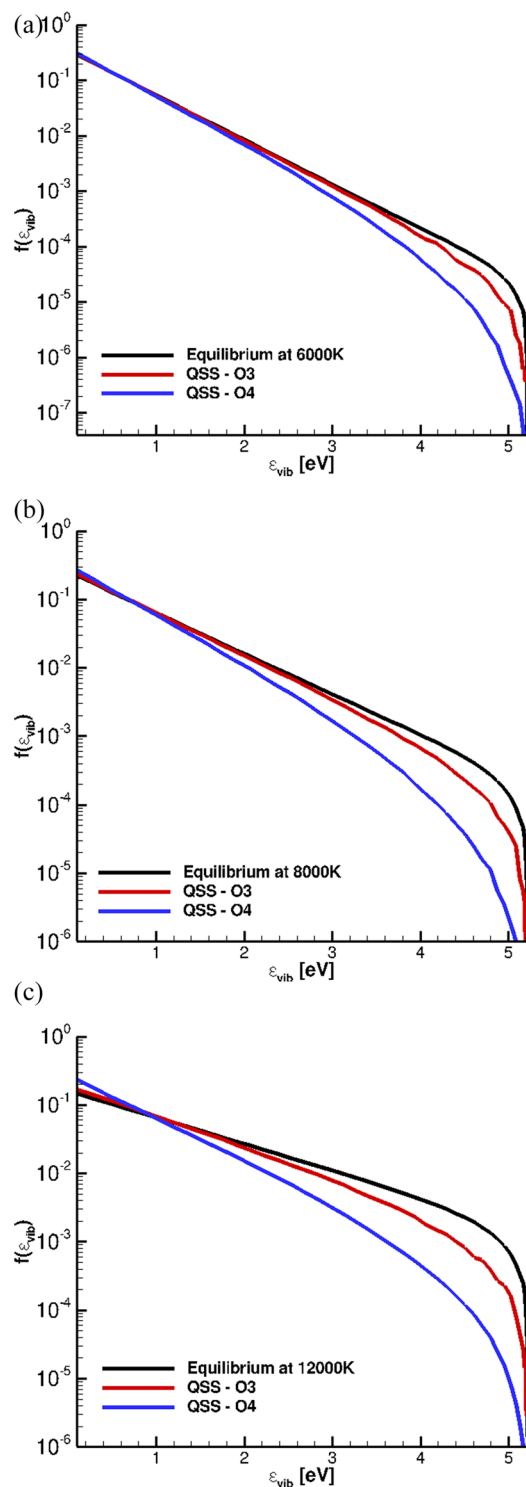


FIG. 10. Comparison of vibrational energy distributions of the system in QSS for separate O_3 (red) and O_4 (blue) systems. Boltzmann distribution at translational temperatures (a) $T = 6000$ K, (b) 8000 K, and (c) $12\,000$ K, respectively (shown in black).

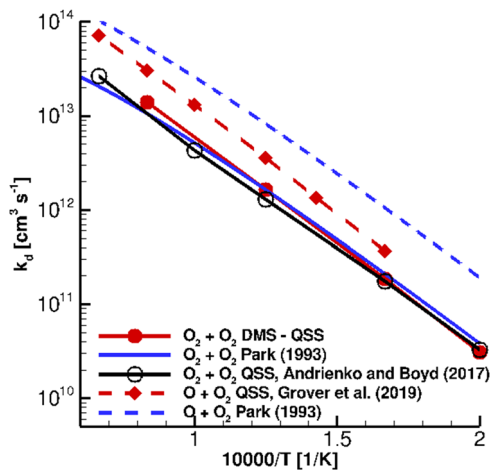


FIG. 11. Comparison of dissociation rate coefficients for oxygen dissociation due to $O_2 + O_2$ interaction and $O + O_2$ interaction obtained by DMS with those proposed by Park² and Andrienko and Boyd.⁵⁵

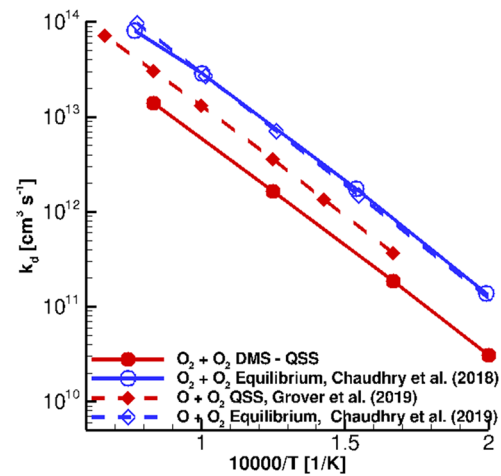


FIG. 12. Comparison of dissociation rate coefficients for oxygen dissociation due to $O_2 + O_2$ interaction and $O + O_2$ interactions under QSS and equilibrium conditions.^{61,72}

the uncertainty in the experimental data is quite large (Fig. 9) and new experiments with lower uncertainty could provide a stronger validation of this finding.

Figure 11 compares the DMS QSS dissociation rate data to the widely used Park model and also compares with O_4 master equation results from the work of Andrienko and Boyd.⁵⁵ (A similar comparison between Andrienko and Boyd's master equation vs our DMS results for the O_3 system can be found in Ref. 37 but is not discussed here.) Although the master equation results for O_4 dissociation appear to agree well with the DMS results, it is important to note that the master equation results did not use a multisurface factor (i.e., $\eta = 1$), and therefore, there is actually a substantial difference in the predictions. Additionally, to characterize O_4 interactions, the master equation analysis required averaging procedures due to the large number of rovibrational transition rates required. Such binning procedures have been shown to significantly affect the predicted dissociation rate coefficients²⁰ for nitrogen. In contrast, the DMS method does not require all transition rates to be precomputed and does not decouple rotational and vibrational energy during the simulation. As a result, the DMS results have minimal assumptions about the internal state of the gas during QSS.

It is important to note that Andrienko and Boyd exclusively used the PES corresponding to the triplet O_4 spin-coupling and hence the results obtained by their analysis only take into account one of the three possible $O_2 + O_2$ interaction types. This implies that in their calculations the triplet O_4 PES was effectively given a statistical weight of 1 instead of the theoretical value of 3/9. Furthermore, the PES used by Andrienko and Boyd⁵⁵ was developed by Varandas and Pais⁷¹ as a PES for O_4 (3A) to study the dynamics of the O (3P) + O_3 (1A_1) reaction. This PES as a subset contains the PES for O_3 in its 1A_1 state⁴⁴ which has been shown to contain spurious features and nonphysical results by Grover *et al.*³⁷

As seen in Fig. 11, the Park model is parameterized such that the rate constant for $O + O_2$ is approximately five times larger than the rate constant for $O_2 + O_2$ collisions. Specifically, the Park model has

$k_d^{O_3}(T_{eff}) = 5 \times k_d^{O_4}(T_{eff})$. Recent QCT calculations indicate that this is incorrect. In fact, QCT calculations⁷² show that for an equilibrium gas initialized with Boltzmann internal energy distributions, that $k_d^{O_3}$ is actually slightly *lower* than $k_d^{O_4}$, as shown in Fig. 12. By combining QCT analysis based on Boltzmann internal energy distributions with DMS analysis involving non-Boltzmann distributions, the factor of two increase in dissociation rate (observed experimentally) is found to be caused entirely by increased vibrational relaxation associated with $O + O_2$ collisions. Although the Park model was developed to empirically capture this factor, the details of the Park model are incorrect and could be improved. Finally, it is noted that similar conclusions have been drawn for nitrogen dissociation using DMS and QCT simulations with *ab initio* PESs.^{7,33,35}

D. Internal energy transfer and dissociation in the full oxygen system

Up until now, we investigated dissociation and vibrational excitation due to $O + O_2$ interactions³⁷ and due to $O_2 + O_2$ interactions, separately. In this section, we analyze isothermal simulations where both $O + O_2$ and $O_2 + O_2$ interactions are enabled. To simulate $O + O_2$ interactions, all nine PESs covering all spin and spatial couplings of the O_3 system are used and, for $O_2 + O_2$ interactions, all three PESs covering all spin couplings of the O_4 system are used. These cases where both $O + O_2$ and $O_2 + O_2$ interactions are allowed simultaneously will be referred to as “full oxygen systems.”

Figure 13 shows the composition and temperature history for full oxygen systems where the translational temperature is $T = 6000$ K [Fig. 13(a)], $T = 10\,000$ K [Fig. 13(b)], and $T = 12\,000$ K [Fig. 13(c)]. The translational temperature is shown in blue, average rotational and vibrational energies divided by the Boltzmann constant are shown in black and red, respectively, and the amount of molecular oxygen remaining in the system as a fraction of the initial value is shown in green. The system was initialized as pure

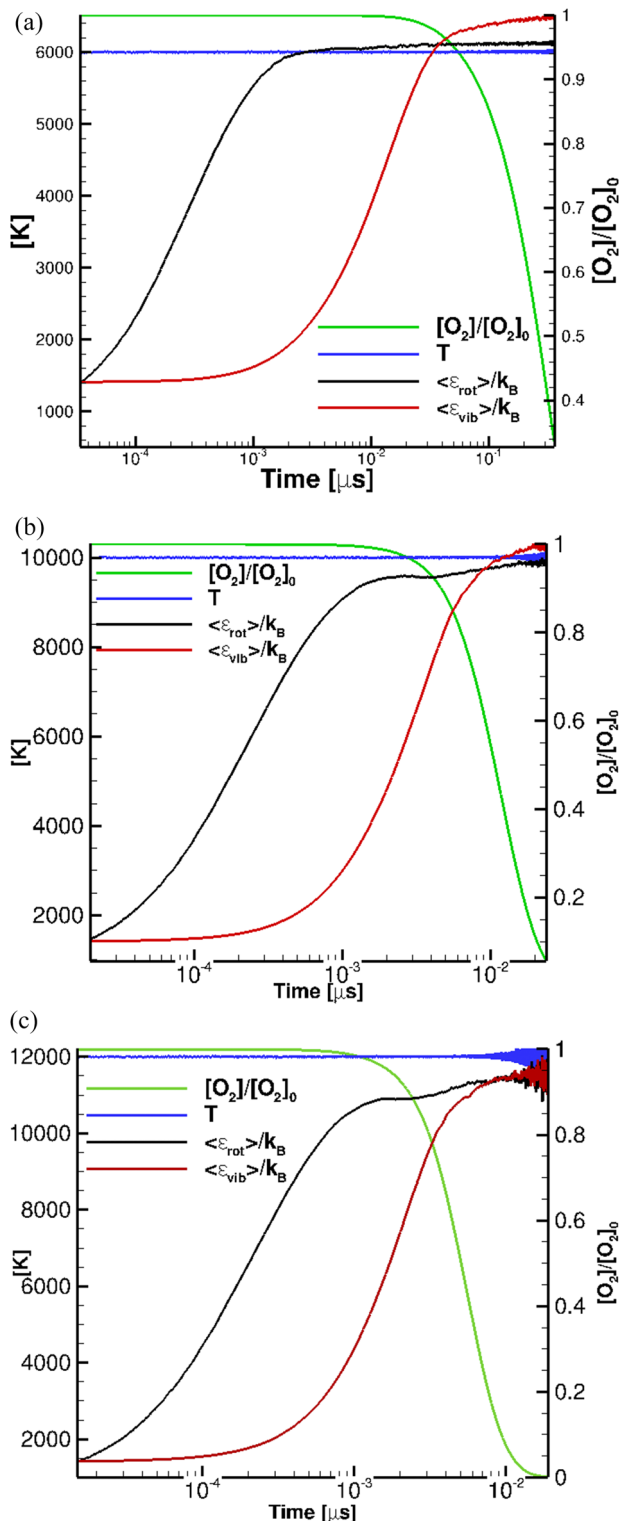


FIG. 13. Composition and temperature history for full oxygen system DMS calculations at reservoir temperatures: (a) $T = 6000 \text{ K}$, (b) $T = 10000 \text{ K}$, and (c) $T = 12000 \text{ K}$.

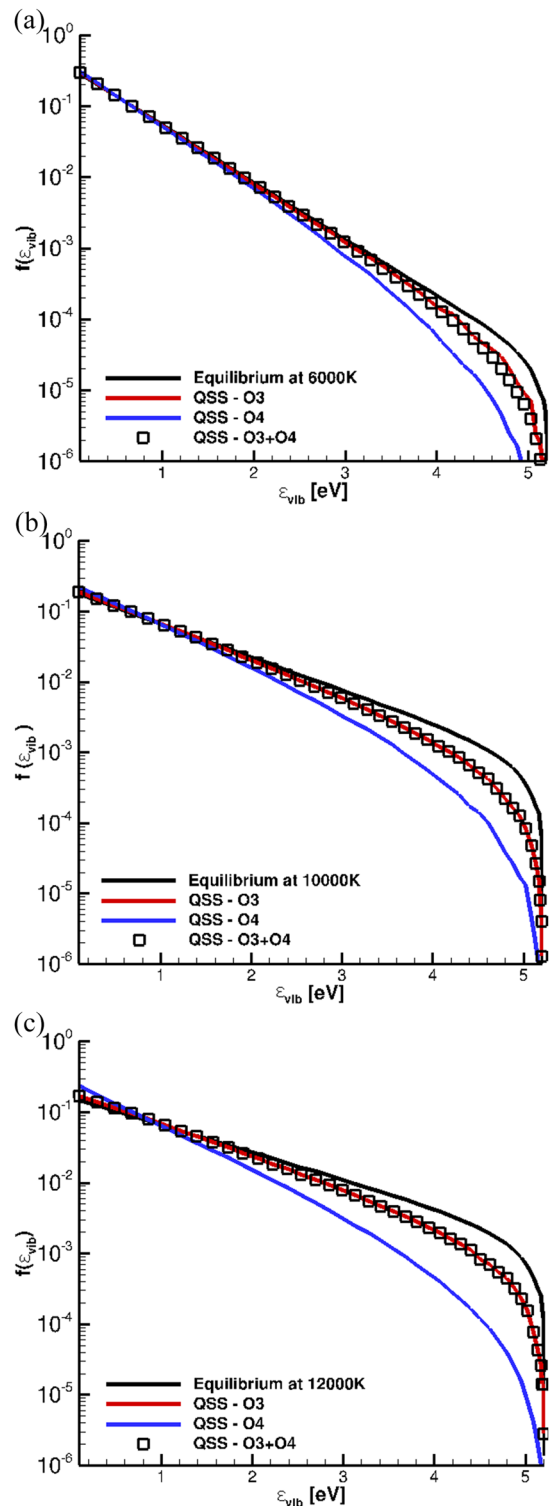


FIG. 14. Comparison of vibrational energy distributions of the system in QSS for the separate O_3 (red line), O_4 (blue line), and combined $O_3 + O_4$ (black squares) systems at reservoir temperatures: (a) $T = 6000 \text{ K}$, (b) $T = 10000 \text{ K}$, and (c) $T = 12000 \text{ K}$.

molecular oxygen with initial rotational and vibrational temperatures set to $\langle \epsilon_{rot} \rangle / k_B = \langle \epsilon_{vib} \rangle / k_B = 1400$ K.

The DMS calculations show the expected trend where rotational energy excitation occurs quickly, followed by vibrational energy excitation and dissociation. The first clear trend to note is the fact that significant dissociation does not occur until the vibrational energy content is sufficiently high. This is evident at each temperature studied and is a strong indication that, at least in the translational temperature range considered here, models should primarily couple dissociation and vibrational energy, rather than rotational energy. The second interesting trend is the “double plateau” in the average rotational energy profile. Since rotational energy excites before any significant dissociation occurs, the rotational energy distribution first reaches a QSS corresponding to the O₄ system. Then, as the vibrational energy increases, dissociation begins, significant atomic oxygen is produced, and the rotational energy excites further toward the QSS corresponding to the O₃ system.

This explanation is further supported by Fig. 14, which plots vibrational energy distribution functions in QSS for the O₄ system, the O₃ system, and the full oxygen system. It is evident that the full oxygen system results in the same QSS distribution as the O₃ system. This is consistent with the fact that during this QSS stage, significant dissociation has already occurred and O + O₂ interactions dominate.

IV. CONCLUSIONS

Internal energy relaxation and dissociation in oxygen is investigated using the direct molecular simulation (DMS) method. DMS is a variant of the DSMC method, where the stochastic collision models are replaced by trajectory calculations using *ab initio* potential energy surfaces (PESs). The sole model input to a DMS calculation is the PES or, in this case, a set of 12 recently constructed PESs that describe O₂ + O₂ and O + O₂ collisions (including all spin-spatial degenerate configurations) in the ground electronic state. DMS calculations predict the expected trends of rovibrational excitation and subsequent dissociation, leading to a quasi-steady-state (QSS) where internal energy excitation is balanced by internal energy loss due to dissociation and internal energy distribution functions exhibit depletion of high-energy states.

In this article, we show that a QSS state is also found in adiabatic DMS calculations and that at a given temperature during the adiabatic calculation, the QSS is found to be the same as that from an isothermal calculation at the same temperature. This was demonstrated at a temperature of T = 6000 K and indicates that isothermal calculations are representative of postshock conditions, where as the gas cools due to dissociation it does so through a series of quasisteady states that can be quantified by isothermal simulations. Similar results have previously been obtained for nitrogen.⁵⁶

Isothermal calculations were performed over a range of temperatures using PESs corresponding to all three spin-couplings of the O₄ system to fully describe O₂ + O₂ interactions. Not much variation was observed for the vibrational energy relaxation among the three PESs describing the O₄ system. The overall vibrational energy relaxation due to O₂ + O₂ interactions agrees closely with Millikan and White⁶⁶ and experimental values.^{62,63,65} Vibrational relaxation due to O₂ + O₂ interactions is also found to be significantly slower than relaxation due to O + O₂ interactions studied in prior work.³⁷

Dissociation rate coefficients in QSS were calculated and lie within the experimental spread. They agree closely with the recent data by Streicher *et al.*,⁶⁵ when it is assumed that dissociation occurs from all excited electronic states below the dissociation limit. A comparison of dissociation in QSS for the O₄ and O₃ system is performed, and it is observed that dissociation in QSS is faster for the O₃ system. This assertion is qualitatively supported by the experimental data of Shatalov.⁶⁷ DMS analysis shows that the increased dissociation observed for O + O₂ interactions can be attributed to the fact that O + O₂ interactions lead to faster vibrational relaxation. In turn, this leads to the vibrational energy distribution being less depleted in QSS when atomic oxygen is present, consequently leading to a higher dissociation rate being observed.

The experimental data combined with the DMS results are a compelling validation that the precise QSS distribution predicted by DMS accurately describes the postshock state of the gas. The DMS results presented in this article can be used to guide the development of new DSMC and CFD models.^{60,72,73}

ACKNOWLEDGMENTS

The research presented was supported by the Air Force Office of Scientific Research (AFOSR) under Grant No. FA9550-16-1-0161. The views and conclusions contained herein are those of the authors and should not be interpreted as necessarily representing the official policies or endorsements, either expressed or implied, of the AFOSR or the U.S. government.

REFERENCES

- H. Hornung, “Induction time for nitrogen dissociation,” *J. Chem. Phys.* **56**, 3172–3173 (1972).
- C. Park, “Review of chemical-kinetic problems of future NASA missions. I: Earth entries,” *J. Thermophys. Heat Transfer* **7**, 385–398 (1993).
- C. Park, “Assessment of a two-temperature kinetic model for dissociating and weakly ionizing nitrogen,” *J. Thermophys. Heat Transfer* **2**, 8–16 (1988).
- C. Park, J. T. Howe, R. L. Jaffe, and G. V. Candler, “Review of chemical-kinetic problems of future NASA missions. II: Mars entries,” *J. Thermophys. Heat Transfer* **8**, 9–23 (1994).
- G. A. Bird, *Molecular Gas Dynamics and Simulation of Gas Flows* (Cambridge University Press, Cambridge, England, 1994).
- D. G. Truhlar and J. T. Muckerman, *Atom-Molecule Collision Theory: A Guide for the Experimentalist* (Plenum Press, New York, NY, 1979), p. 505.
- J. D. Bender, P. Valentini, I. Nompelis, Y. Paukku, Z. Varga, D. G. Truhlar, T. E. Schwartzentruber, and G. V. Candler, “An improved potential energy surface and multi-temperature quasiclassical trajectory calculations of N₂ + N₂ dissociation reactions,” *J. Chem. Phys.* **143**, 054304 (2015).
- G. D. Billing and E. Fisher, “VV and VT rate coefficients in N₂ by a quantum-classical model,” *Chem. Phys.* **43**, 395–401 (1979).
- A. Fernández-Ramos, J. A. Miller, S. J. Klippenstein, and D. G. Truhlar, “Modeling the kinetics of bimolecular reactions,” *Chem. Rev.* **106**, 4518–4584 (2006).
- E. Josyla and W. F. Bailey, “Vibration-dissociation coupling using master equations in nonequilibrium hypersonic blunt-body flow,” *J. Thermophys. Heat Transfer* **15**, 157–167 (2001).
- M. Capitelli, C. M. Ferreira, B. F. Gordiets, and A. I. Osipov, *Plasma Kinetics in Atmospheric Gases* (Springer Science & Business Media, 2013), Vol. 31.
- G. Colonna and M. Capitelli, “Self-consistent model of chemical, vibrational, electron kinetics in nozzle expansion,” *J. Thermophys. Heat Transfer* **15**, 308–316 (2001).
- M. Panesi, R. L. Jaffe, D. W. Schwenke, and T. E. Magin, “Rovibrational internal energy transfer and dissociation of N₂(¹S_g⁺)–N(⁴S_u) system in hypersonic flows,” *J. Chem. Phys.* **138**, 044312 (2013).

- ¹⁴Y. Liu, M. Vinokur, M. Panesi, and T. Magin, "A multi-group maximum entropy model for thermo-chemical nonequilibrium," AIAA Paper 2010-4332, 2010.
- ¹⁵A. Sahai, B. Lopez, C. Johnston, and M. Panesi, "Adaptive coarse graining method for energy transfer and dissociation kinetics of polyatomic species," *J. Chem. Phys.* **147**, 054107 (2017).
- ¹⁶R. L. Macdonald, R. L. Jaffe, D. W. Schwenke, A. Munafò, and M. Panesi, "*Ab initio* based rovibrational grouping model for $N_2(^1\Sigma_g^+)$ – $N_2(^1\Sigma_g^+)$ energy transfer and dissociation," in *47th AIAA Thermophysics Conference* (AIAA, 2017), p. 3164.
- ¹⁷M. Panesi and A. Lani, "Collisional radiative coarse-grain model for ionization in air," *Phys. Fluids* **25**, 057101 (2013).
- ¹⁸E. V. Kustova and E. A. Nagnibeda, "Kinetic model for multi-temperature flows of reacting carbon dioxide mixture," *Chem. Phys.* **398**, 111–117 (2012).
- ¹⁹T. E. Magin, M. Panesi, A. Bourdon, R. L. Jaffe, and D. W. Schwenke, "Coarse-grain model for internal energy excitation and dissociation of molecular nitrogen," *Chem. Phys.* **398**, 90–95 (2012).
- ²⁰R. Macdonald, M. Grover, T. Schwartzentruber, and M. Panesi, "Construction of a coarse-grain quasi-classical trajectory method. II. Comparison against the direct molecular simulation method," *J. Chem. Phys.* **148**, 054310 (2018).
- ²¹R. L. Macdonald, M. S. Grover, T. E. Schwartzentruber, and M. Panesi, "State-to-state and direct molecular simulation study of energy transfer and dissociation in nitrogen mixtures," in *2018 AIAA Aerospace Sciences Meeting* (AIAA, 2018), p. 0239.
- ²²E. Torres and T. E. Magin, "Coupling of state-resolved rovibrational coarse-grain model for nitrogen to stochastic particle method for simulating internal energy excitation and dissociation," *J. Chem. Phys.* **149**, 174106 (2018).
- ²³D. A. Andrienko and I. D. Boyd, "Rovibrational energy transfer and dissociation in O_2 -O collisions," *J. Chem. Phys.* **144**, 104301 (2016).
- ²⁴H. Matsumoto and K. Koura, "Comparison of velocity distribution functions in an argon shock wave between experiments and Monte Carlo calculations for Lennard-Jones potential," *Phys. Fluids A* **3**, 3038–3045 (1991).
- ²⁵K. Koura, "Monte Carlo direct simulation of rotational relaxation of diatomic molecules using classical trajectory calculations: Nitrogen shock wave," *Phys. Fluids* **9**, 3543–3549 (1997).
- ²⁶K. Koura, "Monte Carlo direct simulation of rotational relaxation of nitrogen through high total temperature shock waves using classical trajectory calculations," *Phys. Fluids* **10**, 2689–2691 (1998).
- ²⁷D. Bruno, A. Frezzotti, and G. P. Ghiroldi, "Oxygen transport properties estimation by classical trajectory–direct simulation Monte Carlo," *Phys. Fluids* **27**, 057101 (2015).
- ²⁸D. Bruno, "Direct simulation Monte Carlo simulation of thermal fluctuations in gases," *Phys. Fluids* **31**, 047105 (2019).
- ²⁹P. Norman, P. Valentini, and T. Schwartzentruber, "GPU-accelerated classical trajectory calculation direct simulation Monte Carlo applied to shock waves," *J. Comput. Phys.* **247**, 153–167 (2013).
- ³⁰T. E. Schwartzentruber, M. S. Grover, and P. Valentini, "Direct molecular simulation of nonequilibrium dilute gases," *J. Thermophys. Heat Transfer* **32**, 892–903 (2018).
- ³¹P. Valentini, P. Norman, C. Zhang, and T. E. Schwartzentruber, "Rovibrational coupling in molecular nitrogen at high temperature: An atomic-level study," *Phys. Fluids* **26**, 056103 (2014).
- ³²R. L. Jaffe, D. W. Schwenke, M. Grover, P. Valentini, T. E. Schwartzentruber, S. Venturi, and M. Panesi, "Comparison of quantum mechanical and empirical potential energy surfaces and computed rate coefficients for N_2 dissociation," in *54th AIAA Aerospace Sciences Meeting* (AIAA, 2016), p. 0503.
- ³³P. Valentini, T. E. Schwartzentruber, J. D. Bender, I. Nompelis, and G. V. Candler, "Direct molecular simulation of nitrogen dissociation based on an *ab initio* potential energy surface," *Phys. Fluids* **27**, 086102 (2015).
- ³⁴M. S. Grover, T. E. Schwartzentruber, and R. L. Jaffe, "Dissociation and internal excitation of molecular nitrogen due to N_2 -N collisions using direct molecular simulation," in *55th AIAA Aerospace Sciences Meeting* (AIAA, 2017), p. 0660.
- ³⁵P. Valentini, T. E. Schwartzentruber, J. D. Bender, and G. V. Candler, "Dynamics of nitrogen dissociation from direct molecular simulation," *Phys. Rev. Fluids* **1**, 043402 (2016).
- ³⁶W. Wagner, "A convergence proof for Bird's direct simulation Monte Carlo method for the Boltzmann equation," *J. Stat. Phys.* **66**, 1011–1044 (1992).
- ³⁷M. S. Grover, T. E. Schwartzentruber, Z. Varga, and D. G. Truhlar, "Vibrational energy transfer and collision-induced dissociation in $O + O_2$ collisions," *J. Thermophys. Heat Transfer* **33**(3), 797–807 (2019).
- ³⁸D. Frenkel and B. Smit, *Understanding Molecular Simulation: From Algorithms to Applications* (Academic Press, San Diego, CA, 2002).
- ³⁹Y. Paukku, K. R. Yang, Z. Varga, G. Song, J. D. Bender, and D. G. Truhlar, "Potential energy surfaces of quintet and singlet O_4 ," *J. Chem. Phys.* **147**, 034301 (2017).
- ⁴⁰Y. Paukku, Z. Varga, and D. G. Truhlar, "Potential energy surface of triplet O_4 ," *J. Chem. Phys.* **148**, 124314 (2018).
- ⁴¹Z. Varga, Y. Paukku, and D. G. Truhlar, "Potential energy surfaces for $O + O_2$ collisions," *J. Chem. Phys.* **147**, 154312 (2017).
- ⁴²I. N. Levine, *Quantum Chemistry* (Prentice Hall, Upper Saddle River, NJ, 2000).
- ⁴³R. D. Levine, *Molecular Reaction Dynamics* (Cambridge University Press, Cambridge, England, 2005).
- ⁴⁴A. J. C. Varandas and A. A. C. C. Pais, "A realistic double many-body expansion (DMBE) potential energy surface for ground-state O_3 from a multiproperty fit to *ab initio* calculations, and to experimental spectroscopic, inelastic scattering, and kinetic isotope thermal rate data," *Mol. Phys.* **65**, 843–860 (1988).
- ⁴⁵F. Esposito, I. Armenise, G. Capitta, and M. Capitelli, "O– O_2 state-to-state vibrational relaxation and dissociation rates based on quasiclassical calculations," *Chem. Phys.* **351**, 91–98 (2008).
- ⁴⁶F. Esposito and M. Capitelli, "Quasiclassical trajectory calculations of vibrationally specific dissociation cross-sections and rate constants for the reaction $O + O_2(v) \rightarrow 3O$," *Chem. Phys. Lett.* **364**, 180–187 (2002).
- ⁴⁷M. Kulakhmetov, M. Gallis, and A. Alexeenko, "Effect of $O_2 + O$ *ab initio* and Morse additive pairwise potentials on dissociation and relaxation rates for nonequilibrium flow calculations," *Phys. Fluids* **27**, 087104 (2015).
- ⁴⁸T.-J. Pan, T. J. Wilson, and K. A. Stephani, "Vibrational state-specific model for dissociation and recombination of the $O_2(^3\Sigma_g^+) + O(^3P)$ system in DSMC," *J. Chem. Phys.* **150**, 074305 (2019).
- ⁴⁹I. Borges Sebastião, M. Kulakhmetov, and A. Alexeenko, "DSMC study of oxygen shockwaves based on high-fidelity vibrational relaxation and dissociation models," *Phys. Fluids* **29**, 017102 (2017).
- ⁵⁰R. L. Jaffe, "The calculation of high-temperature equilibrium and nonequilibrium specific heat data for N_2 , O_2 and NO ," in *22nd Thermophysics Conference* (AIAA, 1987), p. 1633.
- ⁵¹R. P. Saxon and B. Liu, "Ab *initio* configuration interaction study of the valence states of O_2 ," *J. Chem. Phys.* **67**, 5432–5441 (1977).
- ⁵²E. E. Nikitin, *Theory of Elementary Atomic and Molecular Processes in Gases* (Clarendon Press, Oxford, 1974).
- ⁵³A. W. Jasper and D. G. Truhlar, "Non-Born–Oppenheimer molecular dynamics for conical intersections, avoided crossings, and weak interactions," in *Conical Intersections: Theory, Computation and Experiment* (World Scientific, 2011), pp. 375–414.
- ⁵⁴D. S. Sholl and J. C. Tully, "A generalized surface hopping method," *J. Chem. Phys.* **109**, 7702–7710 (1998).
- ⁵⁵D. A. Andrienko and I. D. Boyd, "State-specific dissociation in O_2 - O_2 collisions by quasiclassical trajectory method," *Chem. Phys.* **491**, 74–81 (2017).
- ⁵⁶E. Torres and T. E. Schwartzentruber, "Direct molecular simulation of dissociating nitrogen in an adiabatic reactor," in *AIAA SciTech 2019 Forum* (AIAA, 2019), p. 1049.
- ⁵⁷L. Landau and E. Teller, "Zur theorie der schalldispersion," *Phys. Z. Sowjetunion* **10**, 34–38 (1936). [On the theory of sound dispersion, in *Collected Papers of L. D. Landau*, edited by D. ter Haar (Pergamon Press, Oxford, 1965), pp. 147–153 (in English)].
- ⁵⁸R. S. Chaudhry, "Modeling and analysis of chemical kinetics for hypersonic flows in air," Ph.D. thesis, University of Minnesota, Minneapolis, MN, 2018.
- ⁵⁹M. S. Grover, "Direct molecular simulation of nitrogen and oxygen at hypersonic conditions," Ph.D. thesis, University of Minnesota, Minneapolis, MN, 2018.
- ⁶⁰N. Singh and T. E. Schwartzentruber, "Nonequilibrium internal energy distributions during dissociation," *Proc. Natl. Acad. Sci. U. S. A.* **115**, 47–52 (2018).

- ⁶¹R. S. Chaudhry, M. S. Grover, J. D. Bender, T. E. Schwartzentruber, and G. V. Candler, “Quasiclassical trajectory analysis of oxygen dissociation via O₂, O, and N₂,” in *2018 AIAA Aerospace Sciences Meeting* (AIAA, 2018), p. 0237.
- ⁶²L. B. Ibraguimova, A. L. Sergievskaya, V. Y. Levashov, O. P. Shatalov, Y. V. Tunik, and I. E. Zabelinskii, “Investigation of oxygen dissociation and vibrational relaxation at temperatures 4000–10800 K,” *J. Chem. Phys.* **139**, 034317 (2013).
- ⁶³S. A. Losev and N. A. Generalov, “A study of the excitation of vibrations and dissociation of oxygen molecules at high temperatures,” *Sov. Phys. Dokl.* **6**, 1081 (1962).
- ⁶⁴J. H. Kiefer and R. W. Lutz, “The effect of oxygen atoms on the vibrational relaxation of oxygen,” *Symp. (Int.) Combust.* **11**, 67–76 (1967).
- ⁶⁵J. W. Streicher, A. Krish, S. Wang, D. F. Davidson, and R. K. Hanson, “Measurements of oxygen vibrational relaxation and dissociation using ultraviolet laser absorption in shock tube experiments,” in *AIAA SciTech 2019 Forum* (AIAA, 2019), p. 0795.
- ⁶⁶R. C. Millikan and D. R. White, “Systematics of vibrational relaxation,” *J. Chem. Phys.* **39**, 3209–3213 (1963).
- ⁶⁷O. P. Shatalov, “Molecular dissociation of oxygen in the absence of vibrational equilibrium,” *Combust., Explos. Shock Waves* **9**, 610–613 (1973).
- ⁶⁸S. H. Bauer and S. C. Tsang, “Mechanisms for vibrational relaxation at high temperatures,” *Phys. Fluids* **6**, 182–189 (1963).
- ⁶⁹D. L. Thompson, “On a classical trajectory study of energy transfer in some atom-diatomic molecule systems,” *J. Chem. Phys.* **56**, 3570–3580 (1972).
- ⁷⁰M. S. Grover and T. E. Schwartzentruber, “Redistribution of vibrational energy: Mechanisms and transition probabilities,” in *2018 AIAA Aerospace Sciences Meeting* (AIAA, 2018), p. 1231.
- ⁷¹A. Varandas and A. Pais, “Double many-body expansion potential energy surface for O₄(³A), dynamics of the O(³P) + O₃(¹A₁) reaction, and second virial coefficients of molecular oxygen,” in *Theoretical and Computational Models for Organic Chemistry* (Springer, 1991), pp. 55–78.
- ⁷²R. S. Chaudhry and G. V. Candler, “Statistical analyses of quasiclassical trajectory data for air dissociation,” in *AIAA SciTech 2019 Forum* (AIAA, 2019), p. 0789.
- ⁷³N. Singh and T. E. Schwartzentruber, “Coupled vibration-rotation dissociation model for nitrogen from direct molecular simulations,” in *47th AIAA Thermophysics Conference* (AIAA, 2017), p. 3490.